The relationship between pressure drop and liquid saturation in oil-mist filters - predicting filter saturation using a capillary based model

Ryan Mead-Hunter[a,d], Roger D. Braddock[c], Daniel Kampa[b], Nina Merkel[a,b], Gerhard Kasper[b], Benjamin J. Mullins[a,c,d,*]

[a]*Fluid Dynamics Research Group, Curtin University, GPO Box U1987, Perth WA 6845, Australia*

[b]*Institute for Mechanical Process Engineering and Mechanics (MVM), Karlsruher Institut fuer Technologie, D-76131 Karlsruhe, Germany*

[c]*Atmospheric Environment Research Centre, Griffith University, Nathan QLD 4111, Australia*

[d]*Curtin Health Innovation Research Institute, Curtin University, GPO Box U1987, Perth WA 6845, Australia*

Abstract

This work details the results of a study into the relationship between pressure drop and liquid saturation in mist (or coalescing) filters. Liquid saturation (clogging) in mist filters is of critical importance as it is directly related to filter efficiency and flow resistance. Experiments were conducted to determine steady-state saturation and pressure drop values in commonly used oleophillic fibrous filter media, using a range of different combinations of face velocity and number of layers of media within the filter element. Several empirical relationships for saturation and pressure drop were derived based on the relationships found. In addition, a capillary-based saturation model has been described and fitted to the experimental data. A good agreement between the model and data was obtained when an empirically fitted term was added. Equations were developed which allow such variables to be determined from known parameters.

Keywords: Oil-Mist, Filter, Saturation, Pressure drop, Capillary, Wetting, Fibre

*Corresponding author. Telephone +61 8 9266 7029

Email address: b.mullins@curtin.edu.au (Benjamin J. Mullins)

Nomenclature

α packing density

β angle of the fibre to the horizontal

γ surface energy

ΔP Pressure drop

ΔP_c pressure drop through a capillary

ΔP_f Pressure drop, in-line filter

ΔP_T Total pressure drop

ΔP_1 Pressure drop, with adjusted perimeter

ΔP_2 Pressure drop, capillary radius

θ contact angle

θ_r arc angle

μ_g gas viscosity

μ_l liquid viscosity

ξ ratio of pressure drops

ρ_g gas density

σ surface tension

ϕ_x angle of the fibre from the x axis

A_c cross-sectional area of a capillary

Bo the Bond number

Ca the Capillary number

C length of the wetted perimeter

c_f correction to capillary radius

d_f fibre diameter

Dr dimensionless drainage rate term

D drainage rate

h_c height

L_f length of the fibre

N_l number of layers of filter media

P_0 pressure acting on the liquid within the capillary

P_a pressure acting on the liquid surface

r_c capillary radius

S_{Fe} equilibrium filter saturation

S saturation

r_c capillary radius

u gas velocity

V_{oil} volume of oil

V_{void} volume of the void space in the filter

V Volume

W filter width

V_{cs} volume of a slice through a cylinder

x height of liquid

x_∞ equilibrium capillary rise height ($t = \infty$)

x_b height of the capillary that is immersed

Z filter thickness

1. Introduction

The removal of (oil) mists from air streams is important in many industrial applications, such as machining and cutting operations, engine closed crankcase ventilation, and compressed gas cleaning. These mists pose a risk to both the environment and to human health and therefore need to be treated. This is particularly important in factories operating in colder climates, where contaminated air may be recirculated through the building to reduce heating costs. Filters are by far the most efficient devices for removing such particles, however, the filtration of liquid aerosol particles differs so greatly from dust filtration that it is almost a field in itself. This is predominantly due to the ability of the aerosol droplets to coalesce (into larger droplets, liquid columns and arrays of droplets) within the filter, and then to drain from or flow through the filter (which itself is a porous media with a complex structure) under the influence of airflow and gravitational forces.

The presence of the collected liquid in the filter greatly increases the pressure drop of the filter, and (in most cases) has been found to decrease the filtration efficiency, (especially in the diffusional capture regime) [1]. Therefore the accumulated liquid content of a mist filter is of paramount importance, as the saturation influences both pressure drop and collection efficiency. The saturation (S),

$$S = \frac{V_{oil}}{V_{void}}, \tag{1}$$

where V_{void} is the void space in the filter defined as,

$$V_{void} = V(1 - \alpha), \tag{2}$$

and V is the total volume of the filter media and α is the packing density. The saturation is especially critical, since most filter systems operate in a stable flow regime, and the mass loading conditions and will attain a "pseudo"-steady-state. The effect of decreasing the equilibrium saturation (S_e), which is simply the saturation when the "pseudo-"steady-state is attained, will then (usually) be to increase collection efficiency and decrease pressure drop. Achieving improved efficiency and a lower steady-state pressure drop, both of which are pivotal in filter design, will lead to a significant

increase in the filter quality factor (the ratio of collection efficiency to pressure drop) or filter utility factor [2].

While much work has been undertaken on mist filtration [3], [4], [5], [6], [7], [8], [9], very few works have offered models for filter saturation.

The most thorough treatment of equilibrium saturation thus far has been that of Raynor and Leith [10], where empirical equations were derived to allow the prediction of not only saturation but also pressure drop and efficiency. The equilibrium saturation is expressed as,

$$S_{Fe} = \frac{\alpha^{0.39}}{Bo^{(0.47+0.24ln(Bo))}\, Ca^{0.11}} \times exp(-0.04 + 6.6 \times 10^{5} Dr), \qquad (3)$$

with the Bond number (Bo),

$$Bo = \left(\frac{\rho_l g d_f^2}{\sigma}\right) \times 10^{5}, \qquad (4)$$

the Capillary number (Ca),

$$Ca = \left(\frac{\mu_g u}{\sigma}\right) \times 10^{5}, \qquad (5)$$

and the Drainage number (Dr),

$$Dr = \left(\frac{\mu_l D}{\sigma Z W}\right), \qquad (6)$$

where Z is the filter thickness, W is the filter width and D is the drainage rate.

While this work represents an important step forward, it has since been found [11], [12], that Equation 3 is only applicable to filters similar to those used by Raynor and Leith [10], i.e. low packing density, thick media, composed of fibres several microns in diameter. Such filters are not representative of the media used in many modern mist filter systems, which commonly use multiple layers of thin micro fibre glass media (with fibre diameters often an order of magnitude lower than that used by Raynor and Leith [10]); polymer; or stainless steel media.

The main issue with the Raynor and Leith [10] model for such systems, is that equilibrium saturation in finer, denser media has been found [11] to be much more dependant on air velocity than indicated in equation 3.

Frising et al. [11] offer a saturation model that is more complex than the Raynor and Leith [10] model and involves dividing the filter into layers. This model though, does not appear to give better results than the Raynor and Leith [10] model and contains some assumptions which are questionable [13].

Previous work by Mullins et al. [14] and Jaganathan et al. [15] has shown that when commonly used fibrous (mist) filter media are permitted to imbibe liquid (from a reservoir), they behave in a similar manner to a traditional system of vertical capillaries. An additional study [16] examined forced immersion/withdrawal of such media into/from a liquid (oil) bath, and found that such systems could be described by applying a pressure gradient between the top and bottom of the capillary (fibrous media), as is commonly applied in other capillary applications. This work introduced a combined vertical and horizontal capillary model in order to simulate such systems accurately. Yet further work, [17] has found that in modern filter media, altering the airflow velocity acts on saturation in a similar manner to providing a pressure gradient above/below a capillary (increasing airflow velocity decreases S_e and vice versa at a much greater rate than predicted by Equation 3). Bredin and Mullins [17] presented a horizontal capillary model which utilised a distribution of capillary diameters in order to (qualitatively) reproduce the initial saturation profile of a supersaturated/blocked filter being cleaned by airflow

Therefore it can be argued that capillary theory is suitable and appropriate to describe the imbibation of liquid into fibrous filter media when it is in a static state (i.e. without airflow). Also, since the behaviour of an operational mist filter appears to adhere to the general relationship of a capillary system, it should be possible to apply a capillary-based model to describe filter saturation. This work details the results of an extensive series of experiments measuring pressure drop and saturation in microfibre glass and stainless steel media. The work will describe and apply a capillary-based model to determine the capillary rise height in fibrous media whilst air is flowing through the filter. This then will be used to determine steady-state (equilibrium) saturation of the fibrous filter.

2. Capillary Model

Previous work with fibrous filter media [14] determined that, when the Washburn capillary model is used, the effective capillary radius (r_c) can be determined using an empirical function of packing density and fibre radius (r_f). Such that r_c may be described as,

$$r_c = -Aln\left(\frac{\alpha}{r_f}\right) - B, \tag{7}$$

where A and B are material dependent constants [14].

The modified Washburn equation can be written in the following form to incorporate a pressure gradient at the top and bottom of the capillary,

$$\frac{d\left(A_c\rho\left(x-x_b\right)\frac{dx}{dt}\right)}{dt} = \left(P_a - P_0\right)A_c - A_c\rho gx + C\sigma cos\left(\theta\right) - 8\pi\mu\left(x-x_b\right)\frac{d\left(x-x_b\right)}{dt}, \tag{8}$$

where A_c is the cross-sectional area of a capillary, ρ is the density of the liquid, σ is the liquid surface tension, g is acceleration due to gravity,θ is the contact angle, P_a is the pressure acting on the liquid surface, P_0 is the pressure acting on the liquid within the capillary, x is the height of liquid in the capillary and x_b is the height of the capillary that is immersed in liquid.

Once equilibrium has been reached, Equation 8 reduces to,

$$x_\infty = \frac{-\Delta P_c r_c + 2\sigma cos\theta}{r_c\rho g}, \tag{9}$$

where x_∞ is the equilibrium capillary rise height and ΔP_c is the pressure differential between the top and bottom of a vertical capillary. The value of x_∞ can be converted to an overall filter saturation (S or Se) if the geometry of the filter is known. This calculation assumes that all liquid is contained within these theoretical capillaries, and that droplets or films above this fully wetted zone may be neglected. The model assumes that the pressure differential is between the top and bottom of the capillary.

If we consider a fibrous filter, or a series of filters, the total or overall pressure drop between the front and rear faces of the filter can be labelled ΔP_T. If we have a series of filters in-line, then,

$$\Delta P_T = \sum \Delta P_f, \tag{10}$$

for each filter in series. Likewise, we can split a single filter into a series of arbitrary uniform slices in the flow direction, and the overall pressure drop will be the sum of the individual pressure drops for each slice. If the slices are all of the same thickness as $2r_c$ for the media, then

$$\Delta P_T = \sum \Delta P_c, \tag{11}$$

and,

$$\Delta P_c = \omega \Delta P_T, \tag{12}$$

where ω is a dimensionless factor which relates the measured pressure drop between the upstream and downstream sides of the filter to the pressure differential between the top and bottom of the theoretical capillary within the filter, initially assumed $1/n$, where n is the number of slices (equal to the number of capillary diameters from front-rear of the filter)) .

We are of course equating a pressure drop in the flow direction to a capillary pressure across an arbitrary vertical capillary perpendicular to the flow direction, nevertheless, we believe the relationship above is not unrealistic based on experimental observation. As we are modelling a highly porous media as a system of vertical capillaries, the theoretical capillary needs to relate to a "real" capillary within the filters. Examination of the force balance over a capillary at the steady state shows,

$$\Delta P A_c + A_c \rho g x_\infty - C\sigma cos\theta = 0 \tag{13}$$

where A_c is the cross-sectional area of the capillary. Equation 13 may also be expressed in terms of the pressure drop ΔP,

$$\Delta P = \frac{-A_c \rho g x_\infty + C\sigma cos\theta}{A_c}, \tag{14}$$

or substituting πr_c^2 for A_c,

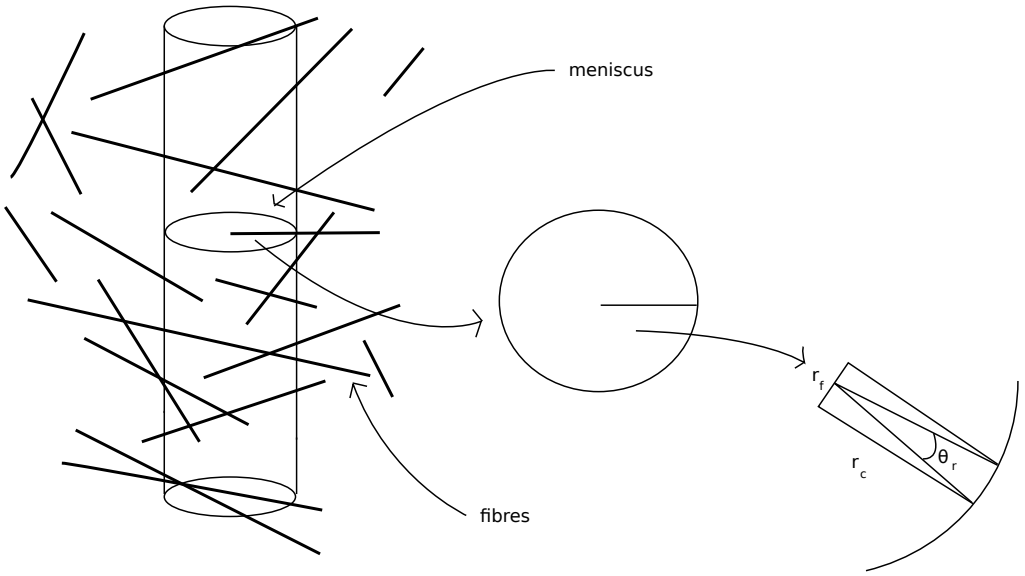

Figure 1: Diagrammatic representation of a cylinder (or theoretical capillary) imposed within the filter media; showing the wetted perimeter when a fibre penetrates at the height of the meniscus

$$\Delta P = \frac{-\pi r_c^2 \rho g x_\infty + 2\pi r_c \sigma cos\theta}{\pi r_c^2}. \tag{15}$$

Examination of Equation 13 reveals that there are two potential variables where deviations from the ideal case (as in the difference between a true capillary and a theoretical 'capillary') may manifest. Firstly, A_c, is dependent on r_c; which in the case of fibrous filters can be described as a function of r_f. The second variable is the wetted perimeter (C).

If a cylinder is visualised within the filter media, it will contain a mixture of free space and fibres, with a packing density comparable to that of the whole filter. At x_∞ the meniscus is described by $C\sigma cos\theta$, for a capillary tube. C is simply the wetted perimeter (such that $C = 2\pi r_c$). However in the case of the theoretical capillary (or cylinder) within the filter media, there will exist fibres which penetrate the cylinder. Taking the simple case of a horizontal fibre penetrating halfway into the theoretical capillary, as illustrated in Figure 1, we can begin to account for the difference in C between the two cases.

There are of course many possible configurations here, given the random orientation of fibres in mist filters. The case illustrated in Figure 1 is chosen for its inherent simplicity; of course one could consider a number of other scenarios; some of which will be mentioned here briefly.

Another model which could be considered is a slice through the cylinder from bottom to top of the meniscus, of height h_c and radius, r_c. This will have a volume (V_{cs}) of

$$V_{cs} = \pi r_c^2 h_c. \tag{16}$$

The volume of filter fibres in this volume will then be

$$\pi r_f^2 L_f = \pi r_c^2 h_c, \tag{17}$$

where L_f is the length of fibre to equate the volume. If the fibre is flat and lies half way into the meniscus, the wetted perimeter is

$$C = 2\pi r_c + (2L_f + 4r_f), \tag{18}$$

where the first term is the circumference of the capillary, and the next two terms are the wetted parts of the fibre along its length, and across the ends. This could be expected to represent an upper value for the circumference, as it only uses a horizontal orientation of the fibre.

Considering then a fibre at angle β to the horizontal, which cuts the horizontal with a cross section of elliptical form, with axes of r_f and $x = r_f/sin(\beta)$. This would require the determination of the circumference of an ellipse, which is described by the integral,

$$C_e = 4r_f \int_0^{\pi/2} \left(\left(\frac{cos(\phi_x)}{sin(\beta)} \right)^2 + (sin(\phi_x))^2 \right)^{\frac{1}{2}} d\phi_x, \tag{19}$$

where ϕ_x is the angle in the fibre from the x axis in normal polar coordinates. This is an elliptic integral, and for $\beta = \pi/2$, this reduces to the circle and gives the correct circumference.

This case is however problematic, as Equation 19 cannot be solved analytically. It would also need to integrated over β to account for all random orientations, and multiplied by the number of fibre crossings of the meniscus volume. While it would be optimal to include all possible permutations in the model, it is evident that it would become extremely complex. Therefore it is the simplest case that will (initially) be explored to see what agreement with the experimental results can be achieved.

Considering then a single fibre oriented horizontally, as illustrated in Figure 1, the value of C may be described as,

$$C = 2\pi r_c - \theta_r r_c + 2r_f + 2(r_c^2 - r_f^2)^{\frac{1}{2}} \tag{20}$$

where θ_r is the angle in radians which defines the arc of the cylinder cross section which is occupied by the penetrating fibre. When the cross sectional area of the capillary is compared to the cross sectional area of a single fibre penetrating the cylinder (where the cylinder wall is assumed to have a thickness of the fibre radius) a result is obtained which is comparable to the filter packing density.

Given that r_f is significantly smaller than r_c, the value of $2(r_c^2 - r_f^2)^{\frac{1}{2}}$ may be approximated by $2r_c$ and the value of $\theta_r r_c$ may be approximated by $2r_f$, which allows Equation 20 to be reduced to,

$$C = 2(\pi + 1)r_c \tag{21}$$

Substituting Equation 21 into Equation 13 a new expression can be developed for the pressure drop, such that;

$$\Delta P_1 = -\rho g x_\infty + \frac{2}{r_c}\frac{(\pi + 1)}{\pi}\sigma cos\theta, \tag{22}$$

where ΔP_1 is the pressure drop with the new (adjusted) wetted perimeter.

Similarly Equation 13 can also be re-written as a function of the fibre radius (i.e. $f(r_f)$), such that;

$$\Delta P_2 = -\rho g x_\infty + \frac{2}{f(r_f)}\sigma cos\theta. \tag{23}$$

Equations 22 and 23 each illustrate the extent to which the changes in the variables will influence the pressure drop experienced by the model 'capillary' in comparison to an actual capillary.

The pressure drops associated with the change in wetted perimeter and the change in the capillary radius may be related to one another by a dimensionless term, ξ, such that:

$$\Delta P_1 = \Delta P_2 \xi, \tag{24}$$

giving;

$$\xi = \frac{\Delta P_1}{\Delta P_2} = \frac{(\pi + 1)}{\pi}\frac{f(r_f)}{r_c} \tag{25}$$

This accounts for both the deviation in the wetted perimeter and the variation in the capillary radius between a capillary and the 'theoretical' capillary. Therefore there is no reason that (given the appropriate function of r_f) Equation 25 should not also be able to be used as our equivalency factor. Thus relating the model 'capillary' to the whole filter; which, as previously demonstrated, generally acts as a capillary system.

By examining Equation 9, it can be seen that when no pressure differential exists, the model will reduce to the modified Washburn equation, from which it is derived, and therefore give the static capillary rise height when both ends of the capillary are at atmospheric pressure. The relationship between the capillary rise height and pressure drop is linear, with the slope affected only by the liquid density, fibre radius and packing density and the intercept (static capillary rise height) is a function of liquid density, surface tension, contact angle, fibre diameter and packing density.

As the pressure drop of a filter is proportional to its thickness, the filter thickness is considered to be an intrinsic property of the pressure drop. Therefore a term for thickness is not utilised in the determination of ω. Equation 9 may

Table 1: Filter and oil properties examined

Filter		Filter Properties			Liquid Properties		
Filter	Material	α	r_f (μm)	z (mm)	Liquid	ρ (kg/m^3)	σ(N/m)
GF1	Glass	0.064	0.55	0.53	Oil A	841	0.028
GF1	Glass	0.064	0.55	0.53	Oil B	875	0.0295
GF2	Glass	0.066	0.32	0.65	Oil A	841	0.028
GF2	Glass	0.066	0.32	0.65	Oil B	875	0.0295
GF3	Glass	0.056	0.31	0.55	Oil A	841	0.028
GF4	Glass	0.054	0.62	0.65	Oil A	841	0.028
GF4	Glass	0.054	0.62	0.65	Oil B	875	0.0295
GF5	Glass	0.0744	0.59	0.39	Oil C	913.4	0.0304
SS1	Steel	0.017	2.2	5.16	Oil B	875	0.0295
SS2	Steel	0.022	2.0	5.08	Oil B	875	0.0295
SS3	Steel	0.016	3.2	6.90	Oil B	875	0.0295

* GF5 data from Frising et al. [11]. This was a 110 mm diameter, circular filter loaded with di-ethyl-hexyl-sebacate (DEHS) (Oil C).

therefore be applied to filters of varying thicknesses and number of layers as used in this work, as well as experimental data from other authors.

3. Experimental

3.1. Materials

Oleophillic glass fibre filter media, produced by Hollingsworth and Vose (H&V, East Walpole, USA), and stainless steel (SS 316) media, produced by Bekaert (Zwevegem, Belgium) were used in the experiments, as they are representative of commonly used industrial mist filter media. The properties of the filter media used in the experiments are shown in Table 1. The filters were either used as single layers, or sandwiched together to form layered filters of up to 5 layers. The filters were tested using both a common laboratory oil, Sigma Light Mineral Oil (Sigma-Aldrich, Australia) (Oil A) and an industrial oil, RX Super (Castrol, Australia) (Oil B). The properties of which are given in Table 1.

The filters used in experiments were either 47 mm circular filters (GF1-GF4), 90x90 mm square filters (GF1-GF4), or cylindrical elements (SS1-SS3) with a height of 90 mm and an inside diameter of 50 mm (using a

coarse supporting mesh on the inside of the cylinder). The different filter chambers (and filter geometries) were utilised to ensure the results were not dependant on filter height. All filters were oriented vertically, with the air flowing horizontally through the media. In the case of the cylindrical elements the flow was from the inside of the cylinder to the outside.

3.2. Experimental Apparatus

The experimental apparatus used for all measurements, is shown in Figure 2. In a typical filter system, the filter media would be saturated gradually by collecting liquid aerosol particles, and may take days or weeks to attain steady-state saturation.

It was found that more rapid saturation of the media could be attained via pre-saturating the media to a higher level than the equilibrium saturation. Rather than slowly accumulating liquid during the experiment, the filter would initially be used in a supersaturated condition, and then slowly drain (or re-entrain) liquid until steady state had been reached. This allowed more rapid experiments and more consistent saturation values between repetitions. However, experiments using aerosol saturation were also performed (and included in the results shown in this work); which included a detailed validation of the dipping method.

To negate the possibility of evaporation of oil during experiments, the influent air was saturated (with the same oil as the test aerosol or filter saturation liquid) before entering the test filter chamber. The air saturator consisted of a chamber packed with coarse, low packing density filter media, saturated with oil, through which air was passed.

High Efficiency Particulate Air (HEPA) filters were placed in front of the filter chamber and the flow meter. The former captured any particles that may have been generated by the saturator, while the latter captured the oil mist re-entrained from the test filter; before it could enter the flow meter.

A manometer (AHJ Systems, Sydney) allowed on-line measurement of the pressure drop across the filter. Particle concentrations before and after the filter were measured using a Scanning Mobility Particle Sizer (SMPS) system consisting of a TSI 3775 Condensation Particle Counter (CPC) and a TSI 3081 Differential Mobility Analyser (DMA). As the majority of experiments were performed using pre-saturated filters, the SMPS was principally used to ensure that the filter was only being challenged with clean (oil vapour saturated) air during these tests.

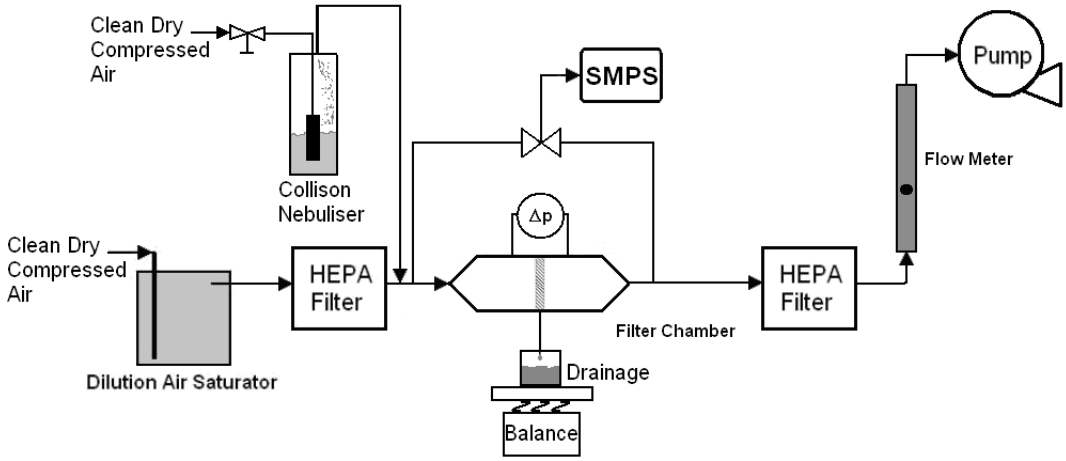

Figure 2: Experimental apparatus

Ten different filter face velocities were used in the experiments (see Section 3.3), which were set via a critical orifice. Not all face velocities were possible to achieve with each filter chamber.

3.3. Experimental Procedure

The filters were either allowed to saturate via collecting aerosol particles over several days (until steady-state pressure drop was reached), or via immersion in a bath of oil. In the "dipped" filter case, the filters were completely immersed in oil for thirty minutes, then removed and allowed to drain for a further thirty minutes, to allow an equilibrium saturation value to be obtained for the no airflow case, which is similar to the maximum value that could be expected in an industrial filter (with no airflow). This saturation level is greater than any equilibrium level which could be attained with air flowing through the filter.

The filter samples (in both clean and saturated conditions) and the filter chamber were weighed before the commencement of each experiment, then again at the end. This allowed the amount of oil in the filter at equilibrium saturation to be determined, as the mass and density of the oil are known

and so Equation 1 can be used.

Four filter face velocities (0.033, 0.153, 0.219 and 0.285 m/s) were used in experiments with glass fibre media, using 1, 2 and 3 layers of filter media for all face velocities, and a select number of 4 and 5 layer experiments with the lowest velocity only. Six filter face velocities (0.267, 0.398, 0.532, 0.663, 0.797 and 0.928 m/s) were used for all stainless steel media experiments. The different filter geometries and filter chambers necessitated different velocities. A minimum of 5 replicate experiments were performed for each media/oil/layer combination.

A number of tests were performed using the same (identical) piece of filter media, with re-saturation between tests, to ensure that the capillarity/pressure drop relationship was reproducible.

4. Results and Discussion

As mentioned previously, the majority of experiments were conducted with pre-saturated aerosol and no influent aerosol loading. This was to allow rapid and easily repeatable experiments, and to exclude loading induced effects (it has been observed that S_e and ΔP_T can increase with increasing aerosol loading in a real filter)

From Figure 3, it can be seen that the dipped and the aerosol saturated filters attained the same ultimate pressure drop, and hence equilibrium saturation, though at different time scales.

Upon commencement of airflow through pre-saturated media samples, ΔP decreased exponentially (and so presumably did S, as it is proportional to ΔP) as the oil drained or re-entrained from the (pre-saturated) filter. It was found that approximately 1 hour was required to reach S_e (defined as $< 1\%$ variation in S and ΔP over 1 hour) for the glass fibre media, and 20 hours for the stainless steel media (due to a significantly larger surface area). These are the times required to reach equilibrium saturation (S_e) with a pre-saturated filter, and would vary depending on the concentration of the aerosol. If the experiments were to be started with a clean filter, loaded conventionally, over 100 hours filtration time would be required. The glass fibre experiments were usually conducted for a minimum of 2 hours duration. Some experiments were however, continued to 12 hours to ensure that the apparent steady state reached at 2 hours was indeed the true steady state. The

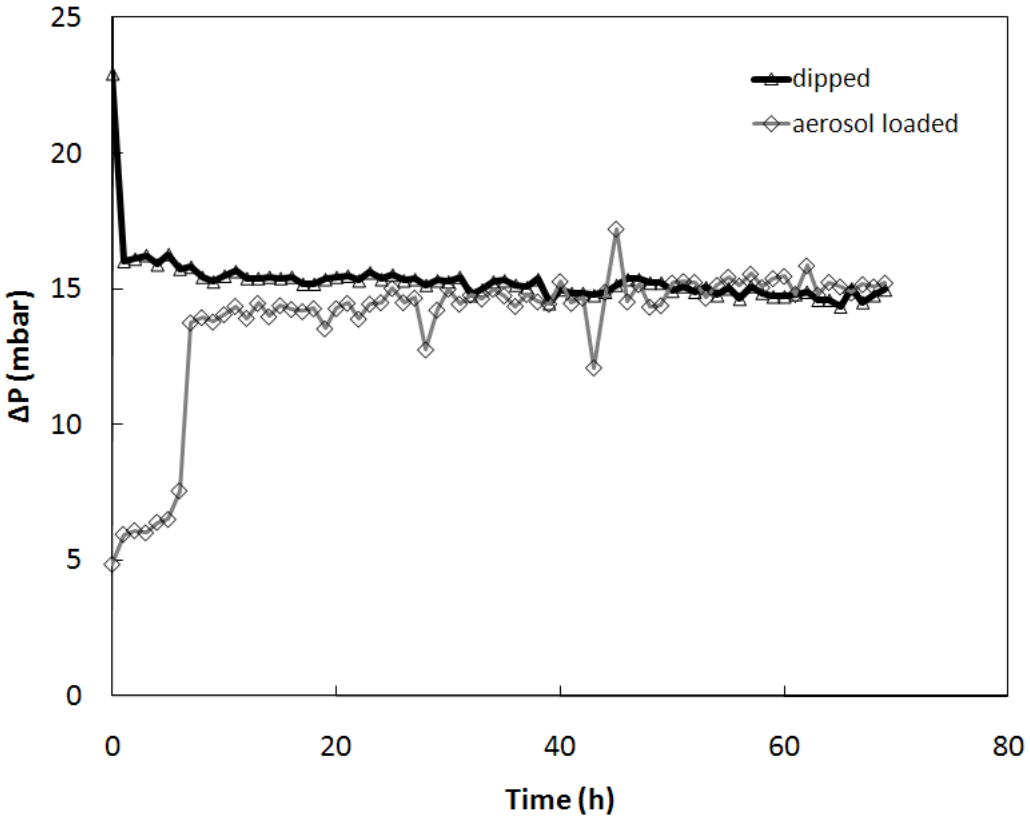

Figure 3: Pressure drop evolution for pre-saturated (dipped) and aerosol saturated SS3 filters

experiments using stainless steel media were generally 40 hours in duration; with some extended to 200 hours.

4.1. Examination of Different Filter Media

The experiments were conducted using 4 different glass-fibre (GF) media and 3 different stainless steel (SS) media (the properties of which, are given in Table 1). Figure 4 shows the equilibrium saturation (S_e) for each of the GF filters, measured in this work, at different filtration velocities and Figure **??** shows the corresponding filter pressure drop.

Figure 4a shows that the GF1 and GF4 are similar and the GF2 and GF3 media are similar in terms of S_e, with the largest difference being between

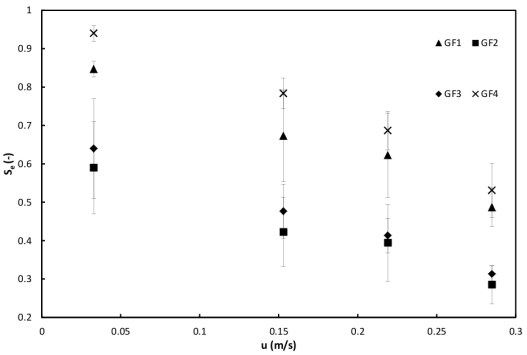

(a)

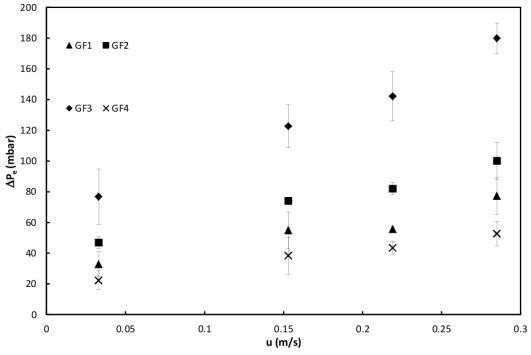

(b)

Figure 4: Equilibrium saturation (a) and pressure drop (b) for single layer GF filters at different velocities (error bars show ± one standard deviation (SD) from the mean)

these two pairs. This may be explained by examination of the filter properties (see Table 1) where, GF2 and GF3 have similar packing density to fibre radius (α/r_f) ratios and GF1 and GF4 posses α/r_f ratios that are closer to each other than they are to those of either GF2 or GF3.

Examination of Figure 4b indicates that the pressure drops for the GF1, GF2 and GF4 filters are closer to each other than any of them are to the GF3 filter. For the GF1, GF2 and GF4 filters the trend may be explained

in terms of the α/r_f ratio, where the pressure drop is higher for filters with higher values of α/r_f. The GF3 filter however, seems to be an exception to this trend. The GF3 filter is however different from the other filters in that it is the only one of the four filters which has both a relatively low packing density and a relatively low fibre radius.

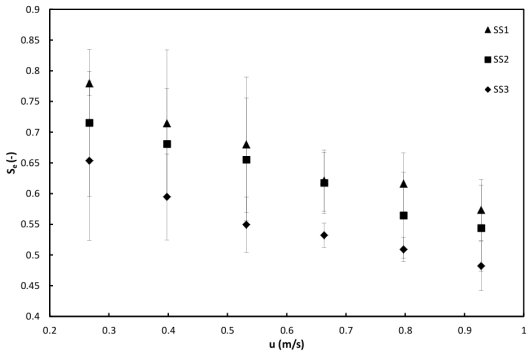

(a)

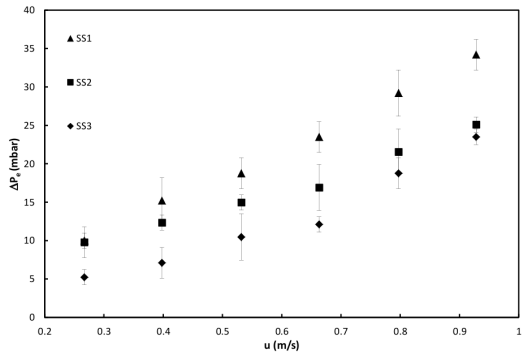

(b)

Figure 5: Equilibrium saturation (a) and pressure drop (b) for SS filters at different velocities (error bars show ± one standard deviation (SD) from the mean)

Each of the data points in Figures 5a and 5b represents a minimum of three measurements. The SS1 and SS3 filters can be seen in both Figures 5a and

5b to follow similar patterns, with the difference between the two likely due to the α/r_f ratio. The SS2 filter behaves slightly differently, though it also has a α/r_f ratio that is significantly higher than that of the SS1 and SS3 filters.

4.2. Examination of Different Layers of Filter Media

Using the GF1 filters and Oil D, the influence of the number of filter layers was investigated. Measurements were carried out on both single and two-layer media, and were attempted on 3-layer media also.

Figure 6a shows the equilibrium saturation reached for each combination of airflow and number of filter layers (for the GF1 filter), while Figure 6b shows the pressure drop for the same experiments (all values are mean ± SD). It was observed, that although the dual-layer filter elements possess a lower S_e than the single layer, the ΔP value is higher for the dual layer; thereby reinforcing the behaviour as a capillary system, where the pressure drop acts to decrease saturation.

For the specific media used in the above experiments, it was possible to derive a simple empirical equation to determine S_e, of the form,

$$S_e = -1.6u - 0.14(N_l - 1) + 1, \tag{26}$$

where N_l is the number of layers of filter media in the element. The R^2 value for the fit to the one layer data is 0.99, for two layers 0.96 and 0.81 for the few samples of 3-layer data (not shown). For all GF filters, a value of S_e=1 will be obtained when u=0. Therefore the equation is expected to be realistic for all such cases, though may not hold for very tall filters, or filters with a lower packing density. Likewise for the equilibrium pressure drop (the pressure drop that corresponds to the equilibrium saturation, ΔP_e), the following relationship could be determined,

$$\Delta P_e = 87N_l u + 10N_l + 20. \tag{27}$$

The R^2 value for one layer is 0.91, for two layers 0.90 and for the three layer

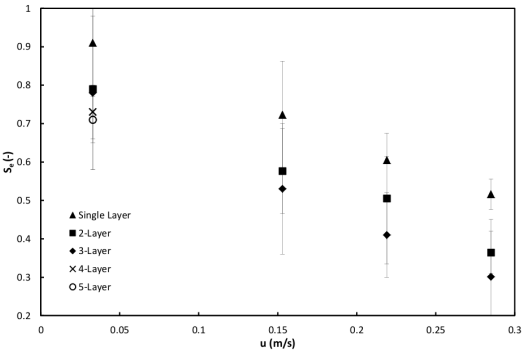

(a)

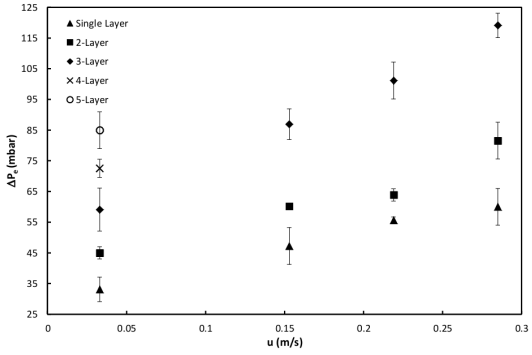

(b)

Figure 6: Equilibrium saturation (a) and pressure drop (b) of GF1 filters as a function of filter face velocity

experiments, 0.69.

When the final pressure from each experiment is plotted against the final saturation of the respective filter (as shown in Figure 7a) a linear correlation can be seen ($R^2 = 0.934$ for the linear fit). In this figure, the results for both one, and two layers of filter media, for all three flow rates, have been included (the three points on the left hand side of the graph are for the 2-layer media, the three points on the right hand side are for the single layer

media). Equation 28 displays the linear fit to Figure 7a, which is fitted to the whole dataset, thus giving a relationship that is independent of the number of layers of media.

$$S_e = -0.0105\Delta P + 1.1939. \tag{28}$$

5. Saturation Model

Initial model calibration determined that if the pressure drop across the (entire) filter (ΔP_e) was utilised, then the model would predict x_∞ (and hence S_e) <0. The coefficient ω was the result of a comparison between a theoretical capillary and a simplified model of filter media.

In order to use Equation 9 it is necessary to select/designate a function of r_f to be used in Equation 25. During the development of Equation 25 a number of scenarios were considered, one of which led to an elliptic integral (Equation 19). While it was the simple case that was chosen, the integral is useful in that it is linear in terms of r_f, which suggests that the function of r_f used in Equation 25 will be linear. It would seem that the simplest function that could be used here would be $f(r_f) = r_f$, which would give an equivalency factor of;

$$\omega = \frac{(\pi + 1)}{\pi} \frac{r_f}{r_c}. \tag{29}$$

The equivalency factor is now expressed as ω as we will be relating the measured pressure drop to an 'equivalent' pressure drop and no longer the pressure drop of a true capillary to our theoretical one. As such the equivalent pressure drop, ΔP_E, can be found using Equation 24. The values of ΔP_E were then used in Equation 9 to find x_∞.

The predicted values of x_∞ were converted to equilibrium saturation (S_e) by simple geometric calculation. (i.e. the volume of the filter accounted for by x_∞ multiplied by the void space $(1 - \alpha)$ of the filter). This method assumes that a sharp boundary exists between the saturated and non-saturated parts of the filter, which may not be the case in some filters [15]. While in the cases presented this sharp boundary was not ideal, in the case of the glass fibre media, the saturated and non-saturated portions could be differentiated

visually, and were sufficiently sharp to be approximated as such in this case.

There is however a deviation between the measured and predicted S_e values, which cannot be explained by altering the value of $f(r_f)$ in Equation 25. This is not unexpected though as it should be remembered that the filter is being modelled as if a system of capillaries. It would therefore seem likely that the capillary radius used in Equation 9 would be subject to some variation (error), and in fact due to the (very) porous nature of the media there is the possibility that a range of effective capillary radii for a particular filter may exist, which can possibly be accounted for by some form of correction to r_c. The capillary radius then becomes;

$$r_c = \left(-A log_e \left(\frac{\alpha}{r_f} \right) - B \right) c_f. \tag{30}$$

As mentioned in Section 2 the values of A and B media-specific constants. These values are also the result of fitting a least squares regression to experimental data with correlation coefficients varying between 0.53 and 0.88 depending on material type [14].

The contact angle (θ) term in Equation 9 does pose a problem however, as it is a dynamic contact angle, and is unable to be determined experimentally for fibrous filters. However, previous work by Mullins et al. [14] determined a range of values for dynamic contact angles, obtained from studies of capillarity in similar or identical fibrous media. They found that the dynamic contact angle fell within the range of 60.7 to 89.3 degrees for all media studied. Similarly Marmur and Cohen [18] found that dynamic contact angles were typically within the range of 71.9 to 76.6 degrees. So setting an initial contact angle within these ranges is not unreasonable. Given that only the intercept of the capillary model will be affected by the contact angle and not the slope, it is possible to use the range of contact angles and the correction factor term for r_c to fit the model.

It can be seen in Figure 7b that a good fit between the model and experimental results could be obtained, demonstrated by an R^2 value of 0.938. Which also serves to validate our choice of function of r_f when determining the equivalency factor.

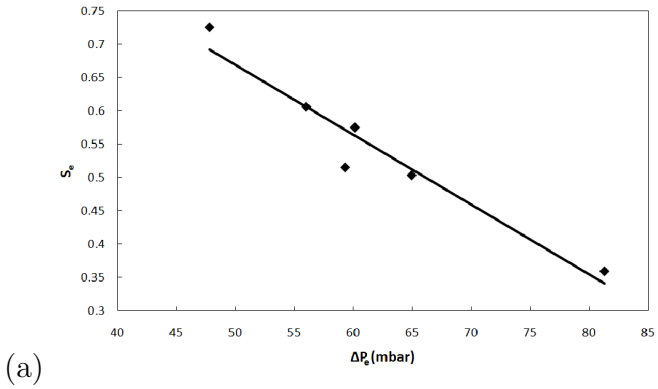

(a)

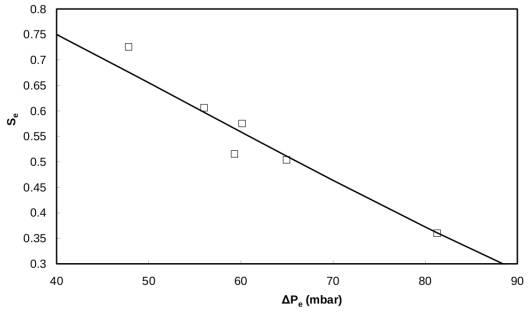

(b)

Figure 7: S_e and ΔP for GF1 filters, using oil A with linear fit added (a). Experimental (symbols) and predicted (solid line) filter saturation S_e as a function of ΔP_e, filter GF1, oil A (b)

It should be noted that it is possible using the capillary model that a value of x_∞ greater than the filter diameter can be obtained. This represents a completely saturated filter and the value of x_∞ cannot be converted to a saturation using a function of filter geometry. This is however allowable as it is entirely possible that for certain fibre radius-packing density combinations that the (theoretical) capillary rise height will be in excess of the filter diameter that is imposed by the filter chamber.

To demonstrate the validity of the model, it was applied (in the same manner) to data corresponding to a range of glass fibre (GF) media and some stainless steel fibre (SS) media tested by the authors for two different oils

Table 2: Filter and model parameter

Filter		Oil	Model		
Filter	Material	Oil	r_c (μm)	c_f	θ
GF1	Glass	Oil D	66.96	0.415	78.2
GF1	Glass	Oil B	66.96	0.415	77.5
GF2	Glass	Oil D	37.94	1	79
GF2	Glass	Oil B	37.94	1	78
GF3	Glass	Oil D	44.66	0.89	75.6
GF4	Glass	Oil D	81.33	0.32	79.1
GF4	Glass	Oil B	81.33	0.32	78.8
GF5	Glass	Oil A	62.88	0.29	71.2
SS1	Steel	Oil B	31.18	0.91	68.8
SS2	Steel	Oil B	22.81	0.98	74.9
SS3	Steel	Oil B	40.16	0.85	68.8

and also fitted to results obtained by Frising et al. [11]. All filter parameters are shown in Table 1. The fitted parameters corresponding to these filters are shown in Table 2.

Figure 8 shows the measured vs predicted data for the combined dataset of GF1-5 and SS1-3 for all different face velocities.

As can be seen in Figure 8 there exists a good fit between modelled and predicted values for the whole dataset ($R^2 = 0.904$). The fit to the glass fibre media alone is further improved at $R^2 = 0.946$. The slight deviation observed in the stainless steel media is likely due to the substantially different packing density-to-fibre radius ratio, which indicates that this media may behave less like a capillary system than the glass fibre media. Nevertheless, all data points in Figure 8 can be seen to fall within $\pm$ 10% of the ideal value. Also, as the conversion to saturation does not take into account the changes in the saturation profile through the thickness of the media, this deviation may be evidence of the effect of neglecting the 'u' shaped saturation profile which is sometimes present in thicker filter media. This effect may need to be accounted for when the thickness of the filter/filter layers exceeds 5mm.

Given the good fit it may be concluded that Figures 7 and 8 demonstrate

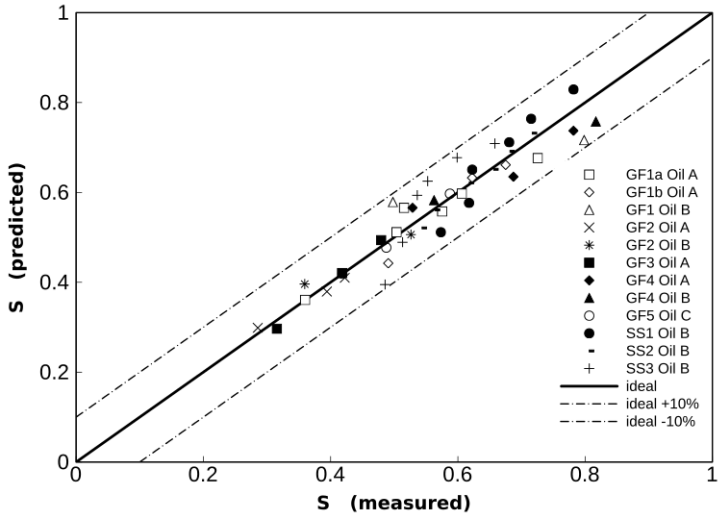

Figure 8: Predicted versus measured equilibrium saturation for all filters

the validity of the model. It also indicates that, as expected, the correction factor is dependent on the filter being used and therefore is a function of one or several properties. If this function can be determined then it should be possible to determine the saturation of a filter for a given pressure drop from easily measurable properties of the filter.

Figure 9 shows the capillary rise height obtained by the modified Washburn equation for varying values of capillary radius and contact angle. It can be observed that increasing θ or decreasing r_c will both decrease x_∞, which should ultimately be the goal in mist filter design.

Using data in Tables 1 and 2, equations for θ and c_f could be determined using generalised linear regression with stepwise backwards elimination. The resultant equations were,

$$\theta = 151.5 - 3.5r_f + 8257\sigma - 0.36\rho \tag{31}$$

and,

$$c_f = 2.0 + 0.4Z - 8.7\alpha - 0.6r_f - 0.04\gamma \tag{32}$$

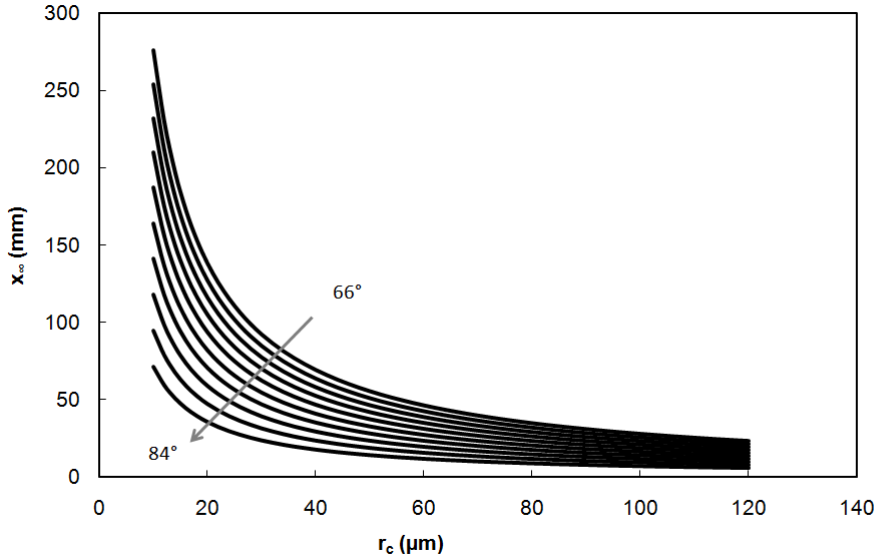

Figure 9: The influence of r_c and θ on x_∞

where γ is the surface energy of the fibre material, and the other parameters are as previously defined. The R^2 values corresponding to the above equations are 0.83 for Equation 31 and 0.87 for Equation 32. It can be observed that θ can be defined in terms of fibre size and fluid properties, which is intuitive, and c_f is a function of filter geometry and fibre surface energy.

Alternatively if the correction factors for the glass fibre filters are plotted against their respective fibre radii there is strong evidence of a linear correlation between the two (see Figure 10). It is known from our results that the correction factor is independent of the oil type used and so it may ultimately be easier to express the correction factor as a function of r_f; as we know that the value of r_c is heavily dependent on r_f. Additionally if there are different correction factors for the different fibre types it will not be necessary to use the surface energy term given by the linear regression. It may also lead to greater accuracy in the model if the fibre materials are treated separately.

Taking this approach the value of c_f for the glass fibre media may be found using the following equation, where the value of R^2 is 0.9702,

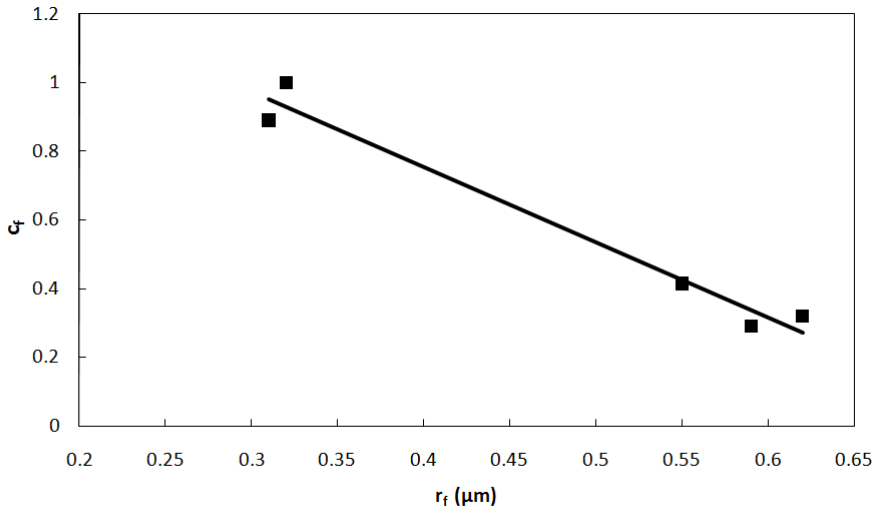

Figure 10: The relationship between the correction factors obtained for the glass fibre media and the fibre radii (with linear fit)

$$c_f = -2.1928 r_f + 1.6312. \tag{33}$$

6. Conclusion

This work has shown that it is possible to determine liquid saturation in single and multi-layer fibrous filter media using an empirically fitted capillary-based model. The work has also detailed several important relationships with respect to saturation and pressure drop in single and multi-layered filter media. However further work is required in order to allow the accurate prediction of the correction factor, which appears to be a function of the fibre diameter.

The model, as it is, will require some experiments to be conducted to allow the model to be calibrated to a new media type. The capillary model detailed within this chapter is applicable to the glass-fibre and stainless steel media used in this work and should also be applicable to similar filters (i.e. those which display significant capillarity and sharp boundaries between wetted and non-wetted areas). In this regard it is potentially of greater efficacy

than the Raynor and Leith [10] model in determining the equilibrium saturation of mist filters.

It is hoped that this work will assist in the advancement of mist filter theory, and the optimisation of such filter systems.

Acknowledgements

This work was supported by an Australian Research Council Linkage Grant (LP0883877).

References

[1] G. M. Letts, P. C. Raynor, R. L. Schumann, Selecting fiber materials to improve mist filters, Journal of Aerosol Science 34 (2003) 1481 – 1492.

[2] A. Podgorski, A. Balazy, L. Gradon, Continuum model evaluation of the effect of saturation on coalescence filtration, Filtech 2005 II (2005) 226–233.

[3] C. Y. Chen, Filtration of aerosols by fibrous media, Chemical Reviews 55 (1955) 595–623.

[4] T. Liew, J. Conder, Fine mist filtration by wet filters–i. liquid saturation and flow resistance of fibrous filters, Journal of Aerosol Science 16 (1985) 497 – 509.

[5] K. W. Lee, B. Y. H. Liu, Experimental study of aerosol filtration by fibrous filters, Aerosol Science and Technology 1 (1981) 35 – 46.

[6] K. W. Lee, B. Y. H. Liu, Theoretical study of aerosol filtration by fibrous filters, Aerosol Science and Technology 1 (1982) 147 – 161.

[7] A. Charvet, Y. Gonthier, E. Gonze, A. Bernis, Experimental and modelled efficiencies during the filtration of a liquid aerosol with a fibrous media, Chemical Engineering Science 65 (2010) 1875–1886.

[8] A. Charvet, S. R. Du Roscoat, M. Peralba, J. F. Bloch, Y. Gonthier, Contribution of synchrotron X-ray holotomography to the understanding of liquid distribution in a medium during liquid aerosol filtration, Chemical Engineering Science 66 (2011) 624–631.

[9] A. Bredin, R. A. OLeary, B. J. Mullins, Filtration of soot-in-oil aerosols: Why do field and laboratory experiments differ?, Separation and Purification Technology 96 (2012) 107 – 116.

[10] P. C. Raynor, D. Leith, The influence of accumulated liquid on fibrous filter performance, Journal of Aerosol Science 31 (2000) 19 – 34.

[11] T. Frising, D. Thomas, D. Bemer, P. Contal, Clogging of fibrous filters by liquid aerosol particles: Experimental and phenomenological modelling study, Chemical Engineering Science 60 (2005) 2751 – 2762.

[12] S. Andan, S. Harihanan, G. Chase, Continuum model evaluation of the effect of saturation on coalescence filtration, Separartion Science and Technology 43 (2008) 1955–1973.

[13] B. J. Mullins, G. Kasper, Comment on: Clogging of fibrous filters by liquid aerosol particles: Experimental and phenomenological modelling study by frising et al., Chemical Engineering Science 61 (2006) 6223 – 6227.

[14] B. J. Mullins, R. D. Braddock, G. Kasper, Capillarity in fibrous filter media: Relationship to filter properties, Chemical Engineering Science 62 (2007) 6191 – 6198.

[15] S. Jaganathan, H. Tafreshi, B. Pourdeyhimi, A realistic modeling of fluid infiltration in thin fibrous sheets, Journal of Applied Physics 105 (2009) 8.

[16] B. J. Mullins, R. D. Braddock, Capillary rise in porous, fibrous media during liquid immersion, International Journal of Heat and Mass Transfer 55 (2012) 6222–6230.

[17] A. Bredin, B. J. Mullins, Influence of flow-interruption on filter performance during the filtration of liquid aerosols by fibrous filters, Separation and Purification Technology 90 (2012) 53–63.

[18] A. Marmur, R. Cohen, Characterization of porous media by the kinetics of liquid penetration: The vertical capillaries model, Journal of Colloid and Interface Science 189 (1997) 299–304.